Simulation Framework for DC Grid Control and ACDC Interaction Studies Based on Modular Multilevel Converters

Simon Wenig, *Student Member, IEEE*, Freiber Rojas, Kevin Schönleber, *Student Member, IEEE*, Michael Suriyah, *Member, IEEE*, and Thomas Leibfried, *Member, IEEE*

***Abstract*—Modular multilevel converter (MMC) topology is discussed intensively as a crucial part of future dc grids, especially to integrate offshore wind power. While generalized voltage-source converter models are usually utilized for multiterminal investigations, conclusions on transient dc grid behavior and on ac–dc interactions during distorted ac grid conditions are hard to draw or are limited in their significance. In this paper, a MMC-based dc grid framework with a tripartite focus on an internal converter as well as dc and ac grid control is presented. Besides, an evaluation of the implemented MMC model that incorporates the available arm sum voltage, a decoupled ac and dc current system control concept that is suitable to handle unbalanced voltage conditions is derived for HVDC applications. Combined with wind farm arrays, this collocation allows a meaningful examination of hybrid ACDC structures and the implemented dc grid control methodologies. To provide proof of the universal applicability of this framework, simulations are carried out on a five-terminal system.**

***Index Terms*—Generalized modular multilevel converter (MMC) modeling, HVDC grid control, MMC energy balancing, power converter, unbalanced operation, wind power integration.**

I. Introduction

THE ONGOING transformation of global power systems toward sustainability is a driving force behind the evolution of high-power voltage-source converter (VSC) development. Challenges to integrate large offshore wind power plants or to increase interelectricity market transfer capabilities have already enabled several link projects across Europe and have triggered research activities to evaluate the feasibility of HVDC grid overlay structures (so called Supergrids) as described in [1]–[3]. The most promising converter topology to meet all essential requirements is the modular multilevel converter (MMC) which was presented in [4] and attracts remarkable interest throughout all fields of power system design and development. The main advantages of a VSC-HVDC system based on MMCs instead of two- or three-level converters are high efficiency and reliability, modularity, superior power quality, the integration of dc-side high-voltage capacitors into distributed arm submodules (SM), reduced or no-filter requirements and compared to line-commutated converters (LCC) the black start capability. In particular, the last two characteristics are of valuable interest for offshore applications due to a smaller converter footprint and a startup of the offshore ac collection grid.

In the long run, regarding also numerous research activities with a focus on hybrid ACDC transmission grid planning and visions of meshed DC overlay networks, a suitable framework to investigate transient system behavior is indispensable. In this context, several challenges arise, as highlighted in a general manner in [5]. These are: 1) model simplification issues for transient multiterminal converter grid investigations, 2) proper converter control concepts to handle system interactions during ac fault scenarios, and 3) external load step changes or contingencies within the dc or one of the connected ac grids from a power system stability perspective.

Since recent HVDC MMC projects consist of a remarkable number of SMs per converter arm of up to several hundred, see [6] for information on the France–Spain link, a reduction of overall computational complexity for a single converter needs to be addressed. If insight into switching device behavior is beyond the intended accuracy, accelerated models allow meaningful results for ac- and dc-side transient investigations as concluded in [7]. It has to be mentioned that these representations and even further reaching steps *a priori* require a practicable highly precise modulation scheme to ensure minimum voltage reference deviations with the smallest possible controller response times. As demonstrated in [8]–[10], this can be assumed.

Various control concepts for the MMC topology exist and have triggered recent summarizing works, see [11]. Following a presupposed straightforward analysis of the converter equivalent circuit and a transformation of the reference variables [10], [12]–[14], independent converter current system control as well as targeted energy balancing techniques can be derived and modified according to the specified field of application. This facilitates strategies to control multiterminal dc grid structures during unbalanced ac grid conditions by buffering unwanted power oscillations in the corresponding converter arm capacitors, thus keeping fluctuations strictly blocked away

Manuscript received November 26, 2014; revised February 11, 2015; accepted March 17, 2015. Date of publication March 30, 2015; date of current version March 22, 2016. This work was supported by the Initiative and Networking Fund of the Helmholtz Association, in the frame of the Helmholtz Energy Alliance "Technologies for the Future Power Grid." Paper no. TPWRD-01438-2014.

S. Wenig, F. Rojas, M. Suriyah, and T. Leibfried are with the Institute of Electric Energy Systems and High-Voltage Technology, Karlsruhe Institute of Technology, Karlsruhe 76131, Germany (e-mail: simon.wenig@kit.edu; freiber.rojas@gmail.com; michael.suriyah@kit.edu; thomas.leibfried@kit.edu).

K. Schönleber is with Electrical Systems, Alstom Renewable Power, Barcelona 08005, Spain (e-mail: kevin.schonleber@power.alstom.com).

Digital Object Identifier 10.1109/TPWRD.2015.2417681

from the dc grid. Investigations with a similar focus to suppress these interactions by adjusting the negative-sequence power output have been carried out in [15]–[18] for single converter and dc-link systems.

This contribution presents an MMC modeling and control concept suitable for transient HVDC grid investigations. Not only does this concern the handling of internal converter currents, but also the active energy level regulation in each converter is considered as an integral part of the concept. Strategies to re-establish power output, grid voltages, and the energy distribution subsequent to grid contingencies differentiate this approach from previous ones. The work is organized as follows: In Section II, the implemented converter model, abstraction steps, and the basic operation principle are described and discussed. Subsequently, Section III identifies the current control loops, while Section IV focuses on the average arm energy control adapted to the dc grid converter role and the handling of unbalanced ac conditions by buffering unwanted power oscillations within the distributed capacitor energy storages. In Section V, dc grid control strategies, the inclusion of offshore wind in feed as well as the converter transformer setting are briefly highlighted. In Section VI, the simulated multiterminal grid and investigated scenarios are introduced and results are shown. Section VII concludes this paper and highlights novel opportunities.

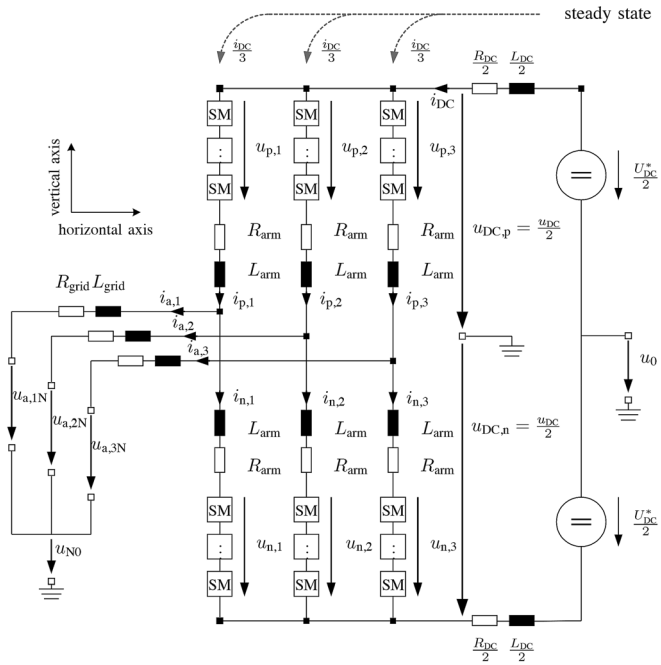

Fig. 1. MMC three phase equivalent circuit connected to an arbitrary ac and dc network.

II. MMC Equivalent Circuit and Arm Modeling

The three-phase MMC topology is composed of six independently controllable m-SM series connections, mostly carried out in a half-bridge SM topology including one capacitor and two insulated-gate bipolar transistor (IGBT) devices. These stacks can be subdivided into three phase modules (y = 1, 2, 3), where each consists of an upper arm (subscript p) and lower arm (subscript n) including associated reactors L_{arm} and occurring resistive losses summarized in R_{arm}. Fig. 1 shows the equivalent circuit, whose parts are analyzed in further detail to derive the basic circuit equations and a suitable control concept including the connected arbitrary ac and dc grid impedance.

A. Equivalent Circuit Analysis

An analysis of ac phase one (a,1) and the corresponding phase module (phm,1) in Fig. 1 leads to the upper and lower loop

$$u_{\mathrm{N0}} + u_{\mathrm{a,1N}} + R_{\mathrm{grid}} \cdot i_{\mathrm{a,1}} + L_{\mathrm{grid}} \cdot \dot{i}_{\mathrm{a,1}} + R_{\mathrm{arm}} \cdot i_{\mathrm{p,1}} + L_{\mathrm{arm}} \cdot \dot{i}_{\mathrm{p,1}} + u_{\mathrm{p,1}} - u_{\mathrm{DC,p}} = 0 \quad (1)$$

and

$$u_{\mathrm{N0}} + u_{\mathrm{a,1N}} + R_{\mathrm{grid}} \cdot i_{\mathrm{a,1}} + L_{\mathrm{grid}} \cdot \dot{i}_{\mathrm{a,1}} - R_{\mathrm{arm}} \cdot i_{\mathrm{n,1}} - L_{\mathrm{arm}} \cdot \dot{i}_{\mathrm{n,1}} - u_{\mathrm{n,1}} + u_{\mathrm{DC,n}} = 0. \quad (2)$$

Applying Kirchhoff's current law, i_{a} can be expressed as

$$i_{\mathrm{a,1}} = i_{\mathrm{p,1}} - i_{\mathrm{n,1}} \quad (3)$$

and, similar to [10], [12], [14], and [19], the phase module current i_{phm} (often also referred to as differential current), can be denoted as

$$i_{\mathrm{phm,1}} = \frac{i_{\mathrm{p,1}} + i_{\mathrm{n,1}}}{2}. \quad (4)$$

Performing $[(1) + (2)]/2$, one obtains the delta current control differential equation

$$\frac{u_{\mathrm{n,1}} - u_{\mathrm{p,1}}}{2} = u_{\mathrm{N0}} + u_{\mathrm{a,1N}} + \left(R_{\mathrm{grid}} + \frac{1}{2}R_{\mathrm{arm}}\right) \cdot i_{\mathrm{a,1}} + \left(L_{\mathrm{grid}} + \frac{1}{2}L_{\mathrm{arm}}\right) \cdot \dot{i}_{\mathrm{a,1}}. \quad (5)$$

In addition, assuming that $u_{\mathrm{DC,p}} = u_{\mathrm{DC,n}} = (u_{\mathrm{DC}})/(2)$, the sum current control differential equation can be derived by performing $[(1) - (2)]/2$ which leads to

$$\frac{u_{\mathrm{p,1}} + u_{\mathrm{n,1}}}{2} = \frac{u_{\mathrm{DC}}}{2} - R_{\mathrm{arm}} \cdot i_{\mathrm{phm,1}} - L_{\mathrm{arm}} \cdot \dot{i}_{\mathrm{phm,1}}. \quad (6)$$

It is apparent that an independent control of ac- and dc-side current systems can be established according to (5) and (6), see also [10]. For simplification issues, we define for the three-phase circuit

$$u_{\Delta,\mathrm{y}} = \frac{u_{\mathrm{n,y}} - u_{\mathrm{p,y}}}{2} \quad (7)$$

$$u_{\Sigma,\mathrm{y}} = \frac{u_{\mathrm{n,y}} + u_{\mathrm{p,y}}}{2}. \quad (8)$$

B. Converter Arm Modeling

For generalized MMC models, a converter arm can be deduced from the power-electronic device level. Depending on the desired degree of accuracy, a tradeoff between modeling depth and computing time has to be made beforehand. Fig. 2 depicts a rough overview of selected approaches, where the first two still rely on individual SM representations with either IGBT devices as indicated in Fig. 2(a), see models Type 1–4 in [20] or, respectively, capacitor-charging level information shown in Fig. 2(b), as proposed in [21] and evaluated in [7]. Thus, their utilization

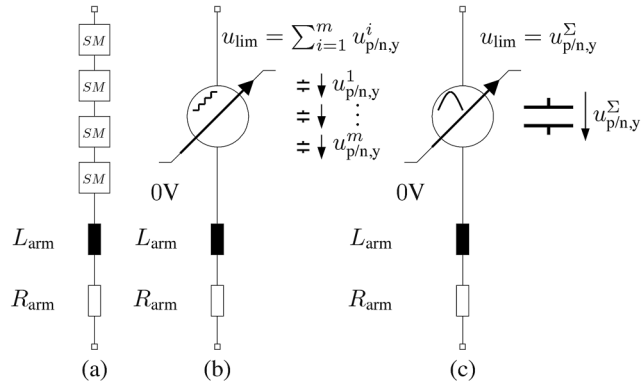

Fig. 2. MMC arm modeling: (a) Detailed SM representation. (b) Modulated source (individual SM voltage representation). (c) Ideal source (sum voltage representation).

requires the implementation of adequate modulation schemes and active cell balancing which ties up a significant share of computational resources and counteracts the idea of a multiterminal dc grid simulation platform for research purposes. However, models that fade out the physical link, see Type 5–6 in [20], neglect internal arm and phase module quantities and mathematically couple ac and dc side instead. This does not fulfill the predefined requirement to allow detailed investigations of ac–dc interactions.

The scope of this paper does explicitly focus on the converter internal current system to investigate the impact of ac grid faults, their propagation and control actions to rebalance the arm energies. This assumes at least a basic insight into global arm quantities, so a fast generalized model is essential. Therefore, the third representation based on an individually adjustable voltage source with maximum voltage limitation is outlined in Fig. 2(c) and embedded in the following simulation works.

Investigating a single arm, the total SM stack energy content is defined by

$$W_{\text{p/n,y}} = \frac{1}{2} \cdot C_{\text{p/n,y}} \sum_{i=1}^{m} \left(u^{i}_{\text{p/n,y}} \right)^2 \tag{9}$$

and changes according to the currently prevailing (instantaneous) arm power

$$p_{\text{p/n,y}} = \dot{W}_{\text{p/n,y}} = u_{\text{p/n,y}} \cdot i_{\text{p/n,y}}. \tag{10}$$

Presupposing an appropriate SM voltage balancing scheme, an equal distribution of the arm sum voltage $u^{\Sigma}_{\text{p/n,y}}$ to the single cells

$$u^{\text{avg}}_{\text{p/n,y}} = \frac{u^{\Sigma}_{\text{p/n,y}}}{m} \tag{11}$$

is valid and spares individual capacitor voltage information. Incorporating this assessment, as addressed and validated in greater detail in [19], we can rewrite (9) as

$$W_{\text{p/n,y}} = \frac{1}{2} \frac{C_{\text{p/n,y}}}{m} \cdot \left(u^{\Sigma}_{\text{p/n,y}} \right)^2. \tag{12}$$

If we now refocus on the arm sum voltage, the following continuous internal arm model can be introduced:

$$u^{\Sigma}_{\text{p/n,y}}(t_1) = \frac{m}{C_{\text{p/n,y}}} \int_{t_0}^{t_1} \frac{p_{\text{p/n,y}}(t)}{u^{\Sigma}_{\text{p/n,y}}(t)} dt + u^{\Sigma}_{\text{p/n,y}}(t_0). \tag{13}$$

This enables a continuous monitoring of the remaining control system influence possibility expressed by the available arm voltage reserve, which is defined as the difference between arm voltage reference requested by the control system and physically available arm sum voltage. In addition, the sum voltage quantities are used to control the energy distribution within the converter. This is valid if all previously discussed requirements are met. Therefore, sum voltage and energy are closely related to each other.

III. MMC Current Control

The continuation of the circuit analysis, which was previously started in Section II-A, is fundamental for the current and later on arm energy balancing control development. By applying the orthogonal stationary reference frame Clarke's Transformation to the extended three-phase sets of (5) and (6), that means to the complete HVDC MMC setting in Fig. 1, the controllable current systems can be obtained.

A. i_{a} Current System

To control the output currents at the ac point of common coupling, the following relations in $\alpha\beta$ are shown:

$$\begin{bmatrix} \dot{i}_{\text{a},\alpha} \\ \dot{i}_{\text{a},\beta} \end{bmatrix} = \frac{1}{L_{\text{grid}} + \frac{1}{2} L_{\text{arm}}} \cdot \begin{bmatrix} u_{\Delta,\alpha} - u_{\text{a},\alpha} - \left(R_{\text{grid}} + \frac{1}{2} R_{\text{arm}} \right) \cdot i_{\text{a},\alpha} \\ u_{\Delta,\beta} - u_{\text{a},\beta} - \left(R_{\text{grid}} + \frac{1}{2} R_{\text{arm}} \right) \cdot i_{\text{a},\beta} \end{bmatrix} \tag{14}$$

can be further transformed into a *dq* rotating frame where independent control of active and reactive power is realized, as widely used in the literature.

Depending on the converter ac grid connection, which will be discussed in more detail in Section V.C, the $i_{\text{a},0}$ component is blocked away from the converter by implementing an appropriate transformer. Due to this reason, this current control loop is void.

B. i_{phm} Current System

Following an equal methodology to analyze the phase module current loops, an internal converter current system is obtained. It is obvious that

$$\begin{bmatrix} \dot{i}_{\text{phm},\alpha} \\ \dot{i}_{\text{phm},\beta} \end{bmatrix} = \frac{1}{L_{\text{arm}}} \begin{bmatrix} -u_{\Sigma,\alpha} - R_{\text{arm}} \cdot i_{\text{phm},\alpha} \\ -u_{\Sigma,\beta} - R_{\text{arm}} \cdot i_{\text{phm},\beta} \end{bmatrix} \tag{15}$$

has no effect on the attached arbitrary dc network and represents internal quantities that do not affect the converter terminals. An external dc-side power exchange is strictly realized by adjusting the phase module $i_{\text{phm},0}$ component. To deduce the connection between this current and the dc network, we replace u_{DC} in Fig. 1 with

$$u_{\text{DC}} = U^{*}_{\text{DC}} - R_{\text{DC}} \cdot i_{\text{DC}} - L_{\text{DC}} \cdot \dot{i}_{\text{DC}} \tag{16}$$

and rewrite the current i_{DC} as

$$i_{\mathrm{DC}} = 3 \cdot i_{\mathrm{phm},0}. \tag{17}$$

This leads to the $i_{\mathrm{phm},0}$ control loop to adjust the dc-side power exchange, which is given as

$$\left[\dot{i}_{\mathrm{phm},0}\right] = \frac{1}{L_{\mathrm{arm}} + \frac{3}{2}L_{\mathrm{DC}}} \cdot \left[-\frac{U^*_{\mathrm{DC}}}{2} - u_{\Sigma,0} - \left(R_{\mathrm{arm}} + \frac{3}{2}R_{\mathrm{DC}}\right) \cdot i_{\mathrm{phm},0}\right]. \tag{18}$$

IV. Unbalanced Voltage Condition Handling and Average Energy Control

In addition to steady-state operation, ac grid-interfaced converters have to withstand unbalanced voltage conditions and permanently track grid frequency deviations. Especially in the scope of multiterminal dc grid control strategy development, interactions which affect the dc side must be avoided or at least minimized.

A. Unbalanced Voltage Conditions

The implementation of single reference frame phase-locked loop techniques show limited performance during dynamic events; therefore, a reliable and fast positive-/negative-sequence estimation is essential. As proposed in [22] and evaluated from a design-oriented perspective in [23], the multiple complex coefficient filter (MCCF) structure provides the desired functionality, which includes an accurate sequence detection with unity gain as well as zero phase shift and is also extendable to detect selected harmonic components. The ac grid-side voltages $u_{\mathrm{a,y}}$ and the converter voltages $u_{\Delta,\mathrm{y}}$ can be separated into positive- and negative-sequence parts. If we neglect u_{N0} and summarize $R = (R_{\mathrm{grid}} + (1)/(2)R_{\mathrm{arm}})$, $L = (L_{\mathrm{grid}} + (1)/(2)L_{\mathrm{arm}})$, we can rewrite (5) as

$$u^{+}_{\Delta,\mathrm{y}} = u^{+}_{\mathrm{a,yN}} + R \cdot i^{+}_{\mathrm{a,y}} + L \cdot \dot{i}^{+}_{\mathrm{a,y}} \tag{19}$$

and

$$u^{-}_{\Delta,\mathrm{y}} = u^{-}_{\mathrm{a,yN}} + R \cdot i^{-}_{\mathrm{a,y}} + L \cdot \dot{i}^{-}_{\mathrm{a,y}}. \tag{20}$$

where $+$ and $-$ denote the positive- and negative-sequence components. An individual sequence control can be either realized by transforming these relations into two oppositely rotating *dq* reference frames, or if the negative-sequence current components are supposed to be eliminated, such as in [16], the negative-sequence voltage is directly fed through from the MCCF. This leads to the fact that there is no negative-sequence voltage difference; therefore, ac currents are kept balanced during single-line faults.

B. Average Arm Energy Control

As highlighted in Section II-B, the arm energies $W_{\mathrm{p/n,y}}$ are related to the corresponding sum voltages $u^{\Sigma}_{\mathrm{p/n,y}}$. The latter value, in turn, is separated into an average $\bar{u}^{\Sigma}_{\mathrm{p/n,y}}$ and an alternating $\tilde{u}^{\Sigma}_{\mathrm{p/n,y}}$ component, assuming $\tilde{u}^{\Sigma}_{\mathrm{p/n,y}} \ll \bar{u}^{\Sigma}_{\mathrm{p/n,y}}$ we can rewrite (12)

$$W_{\mathrm{p/n,y}} = \frac{1}{2} \cdot \frac{C_{\mathrm{p/n,y}}}{m} \cdot \left(\bar{u}^{\Sigma}_{\mathrm{p/n,y}} + \tilde{u}^{\Sigma}_{\mathrm{p/n,y}}\right)^2 \approx \frac{1}{2} \cdot \frac{C_{\mathrm{p/n,y}}}{m} \cdot \left(\bar{u}^{\Sigma}_{\mathrm{p/n,y}}\right)^2. \tag{21}$$

To maintain the converter arm quantities within the operational boundaries, the relation between arm power and sum voltage

$$p_{\mathrm{p/n,y}} = \dot{W}_{\mathrm{p/n,y}} = \frac{C_{\mathrm{p/n,y}}}{m} \cdot \bar{u}^{\Sigma}_{\mathrm{p/n,y}} \cdot \frac{du^{\Sigma}_{\mathrm{p/n,y}}(t)}{dt} \tag{22}$$

which is linearized at $u^{\Sigma}_{\mathrm{p/n,y}} = \bar{u}^{\Sigma}_{\mathrm{p/n,y}}$ is derived, where we can replace

$$p_{\mathrm{p/n,y}} = (u_{\Sigma,\mathrm{y}} \mp u_{\Delta,\mathrm{y}}) \cdot \left(i_{\mathrm{phm,y}} \pm \frac{i_{\mathrm{a,y}}}{2}\right) \tag{23}$$

for the detailed analysis. For the active regulation, we define $p_{\Sigma,\mathrm{y}}$, $p_{\Delta,\mathrm{y}}$ power and sum voltage $u^{\Sigma}_{\Sigma,\mathrm{y}}$, $u^{\Sigma}_{\Delta,\mathrm{y}}$ components similar to the ones in (7) and (8) and perform Clarke's transformation as shown in [10] and [12]. The overall balancing concept, which can be split into a total, horizontal, and vertical task (see Fig. 1 for the axes definition), is then based on the expressions

$$\frac{C_{\mathrm{p/n,y}}}{m} \cdot \bar{u}^{\Sigma}_{\mathrm{p/n,y}} \cdot \begin{bmatrix} \dot{u}^{\Sigma}_{\Sigma,\alpha} \\ \dot{u}^{\Sigma}_{\Sigma,\beta} \\ \dot{u}^{\Sigma}_{\Sigma,0} \end{bmatrix} = \begin{bmatrix} p_{\Sigma,\alpha} \\ p_{\Sigma,\beta} \\ p_{\Sigma,0} \end{bmatrix} \tag{24}$$

and

$$\frac{C_{\mathrm{p/n,y}}}{m} \cdot \bar{u}^{\Sigma}_{\mathrm{p/n,y}} \cdot \begin{bmatrix} \dot{u}^{\Sigma}_{\Delta,\alpha} \\ \dot{u}^{\Sigma}_{\Delta,\beta} \\ \dot{u}^{\Sigma}_{\Delta,0} \end{bmatrix} = \begin{bmatrix} p_{\Delta,\alpha} \\ p_{\Delta,\beta} \\ p_{\Delta,0} \end{bmatrix}. \tag{25}$$

Instead of instantaneous values, the average arm power value is regulated by integrating a grid period averaging filter. Either a lowpass with a cutoff frequency ω_{c} smaller than the grid frequency ω_{g} or a finite-impulse-response (FIR)-type filter provides the specified characteristics. As a direct consequence of controlling the average arm energy content and the additional possibility to adjust ac- and dc-side currents independently, inherently present capacitor sum voltage ripples with a double-line frequency as well as active power oscillations caused by unbalanced voltage conditions do not lead to an immediate balancing control action. This fact avoids the direct propagation of fluctuations or disturbances from an interfaced ac grid into the connected dc system. Assuming an operation point

$$\begin{bmatrix} u_{\Sigma,\alpha} \\ u_{\Sigma,\beta} \\ u_{\Sigma,0} \end{bmatrix} = \begin{bmatrix} 0 \\ 0 \\ \frac{u_{\mathrm{DC}}}{2} \end{bmatrix} \tag{26}$$

the following relations can be identified:

1) Total Energy Balancing: According to its role within a meshed dc network, a converter terminal can change its power transfer either on the ac- or dc-side terminals individually to adjust the total system energy level, and a brief introduction follows in Section V. Analyzing $p_{\Sigma,0}$ given in (24) by inserting the detailed representations of $p_{\mathrm{p/n,y}}$ described in (23) leads to

$$p_{\Sigma,0} = u_{\Sigma,0} \cdot i_{\mathrm{phm},0} - \frac{1}{4}\left(u_{\Delta,\alpha} \cdot i_{\mathrm{a},\alpha} + u_{\Delta,\beta} \cdot i_{\mathrm{a},\beta}\right). \tag{27}$$

Depending on the preferred orientation of the power adjustment, we have to either adapt $i_{\mathrm{phm},0}$ or $i_{\mathrm{a},\alpha}$ and $i_{\mathrm{a},\beta}$. However, overall control scheme signal routing and control gain identification due to the different time constants of the control loops have to be taken into account.

2) Horizontal Energy Balancing: In case of a distortion between the phase module energy levels, referred to as horizontal

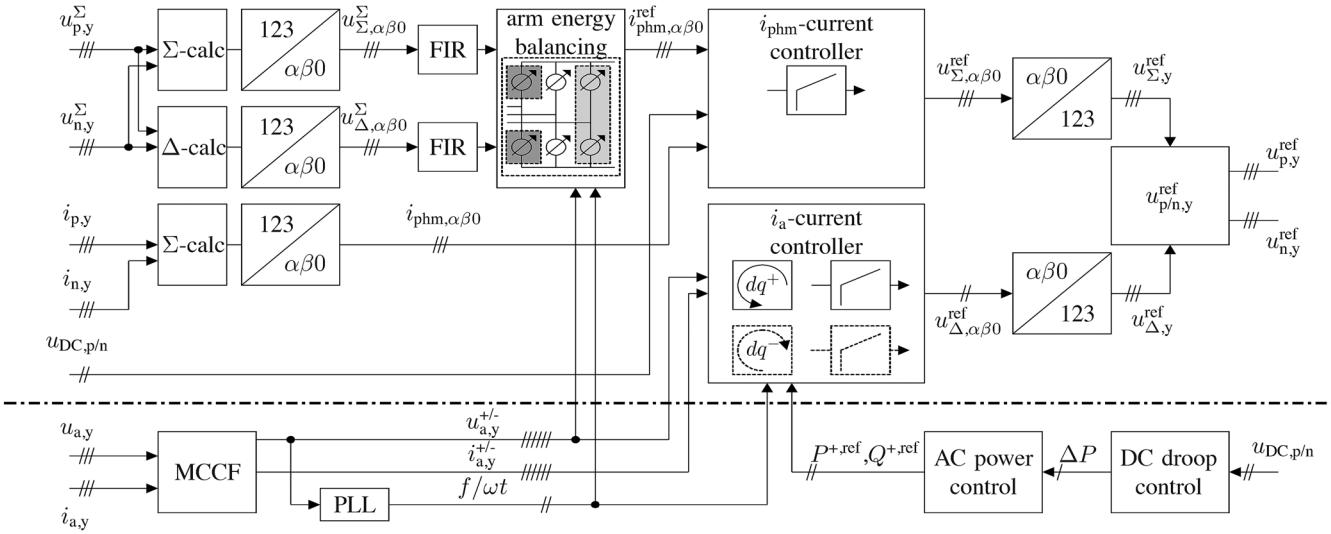

Fig. 3. Schematic overview of the embedded control scheme for an ac grid-interfaced MMC with droop control.

balancing task in the following, it is superior to adjust the converter internal currents since a change of ac-side quantities leads to unbalanced line currents. The power component is defined with

$$\begin{bmatrix} p_{\Sigma,\alpha} \\ p_{\Sigma,\beta} \end{bmatrix} = \begin{bmatrix} u_{\Sigma,0} \cdot i_{\mathrm{phm},\alpha} - \frac{1}{4} u_{\Delta,\alpha} \cdot i_{\mathrm{a},\alpha} + \frac{1}{4} u_{\Delta,\beta} \cdot i_{\mathrm{a},\beta} \\ u_{\Sigma,0} \cdot i_{\mathrm{phm},\beta} - \frac{1}{4} u_{\Delta,\alpha} \cdot i_{\mathrm{a},\beta} + \frac{1}{4} u_{\Delta,\beta} \cdot i_{\mathrm{a},\alpha} \end{bmatrix} \tag{28}$$

so an internal current system direct-current component in $i_{\mathrm{phm},\alpha\beta}$ causes the aspired active power adjustment.

3) Vertical Energy Balancing: An equal energy distribution between the upper and lower arm of each phase module without affecting the clamp currents can be realized by modifying the delta power components $p_{\Delta,\alpha\beta 0}$ given in (25). As explained in a straightforward manner in [12], internal converter currents $i_{\mathrm{phm},\alpha\beta}$ containing grid frequency components are suitable to generate an active power transfer in the vertical direction by taking advantage of the fact that the upper and lower arm three-phase voltage systems are phase shifted by 180°.

C. Schematic Control Scheme

The overall control system structure is visualized in Fig. 3. The upper part shows, from left to right, sum voltage and arm current measurement and transformation, grid period average energy control, and the phase module current controller, which provides the $u^{\mathrm{ref}}_{\Sigma,\mathrm{y}}$ arm reference voltage components. In addition, the MCCF quantities measured at the ac point of common coupling and the converter dc-side voltages lead to the $u^{\mathrm{ref}}_{\Delta,\mathrm{y}}$ reference components which affect the ac-side power transfer.

V. Multiterminal DC Including Offshore Wind

This section briefly highlights, in addition to the presented converter control concept, dc grid control strategies, offshore wind integration, as well as the collection grid layout and suitable topologies for converter transformers.

A. DC Grid Control Strategies

Simple and advanced droop control methods are inevitably connected to reliable and secure dc system operation since no real-time communication is required during primary control actions. The classification of several grid converter roles and situational response curves, see [24], enables continuous operation in case of individual converter setpoint changes, short-circuit scenarios in one of the interfaced ac networks, or a converter failure. As described in [25] and validated in [26] for simplified VSC converter structures, similar to the model in [27], multiterminal systems can be controlled using either centralized (one single u_{DC} controlled terminal) or decentralized (several droop $P = f(u_{\mathrm{DC}})$ terminals) approaches. In case of an outage, one terminal may be assumed to undertake the master balancing task inherited from the previously responsible stations or several terminals share the burden in case of a large disturbance not to overstress a single-interfaced ac system. This is realized by a sequentially designed simple droop in combination with deadband droop strategies.

B. Offshore Rectifier and Collection Grid

The offshore converter must absorb the available power fed in from the wind turbines, see [29] and [30], which is realized with an ac voltage magnitude controller. Technical parameters for the following simulations, such as collection grid voltage, layout, and reactive power compensation are oriented on the overview presented in [31].

C. Converter Transformer

To ensure that no ac zero-sequence current propagates into the dc system and affects system behavior, converter transformers for high-voltage applications are carried out in a star-delta configuration and ensure $i_{\mathrm{a},1} + i_{\mathrm{a},2} + i_{\mathrm{a},3} = 0$. Alternatives, such as the one presented in [32], tackle the problem from another perspective, but do not offer beneficial symmetrizing characteristics during one or two phase faults

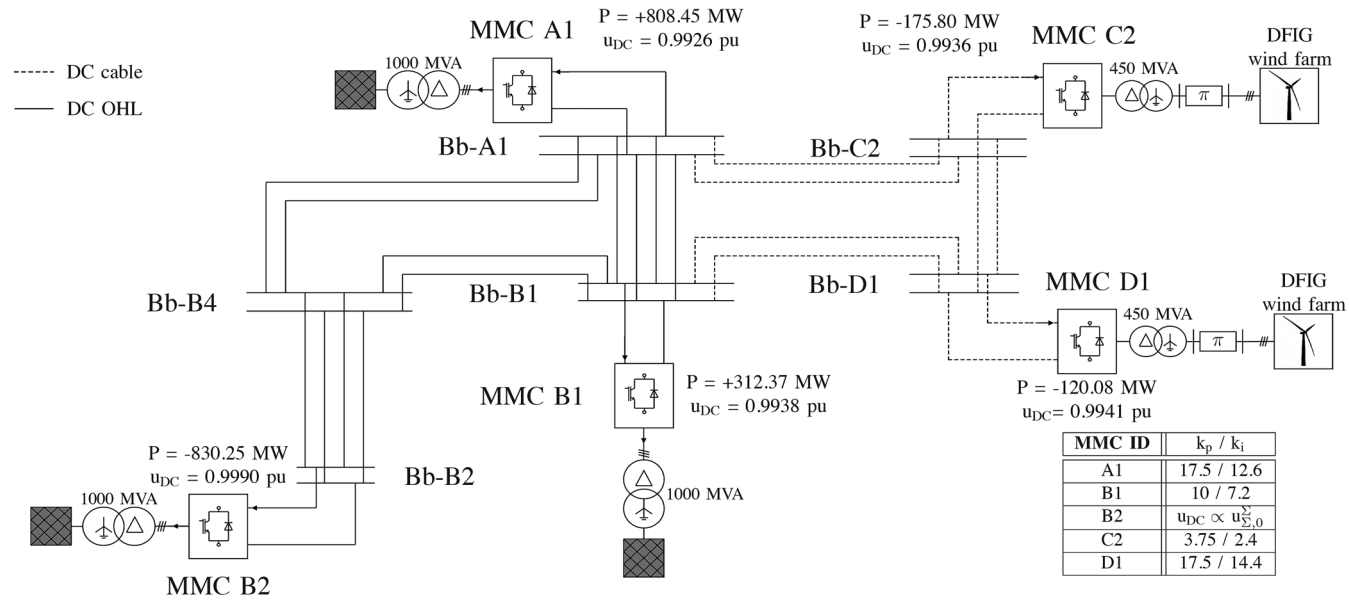

Fig. 4. Five-terminal dc grid scenario related to the DCS3 subsystem introduced in [28] including initial load-flow values for each terminal at $t = 3$ s.

so the interfaced components are subject to higher stress. For this reason, a star-delta transformer setting is chosen for the following investigations.

VI. Scenario and Simulation Results

This section introduces grid topology and the main parameters of the investigated multiterminal dc system. Simulations are carried out in Matlab/Simulink where a fixed step solver with a time step of 25 μs is applied. The step size is chosen according to considerations provided in [5] and takes into account the controller sample time of 50 μs. A positive power value represents an ac side in feed.

A. Multiterminal DC Grid Configuration

As visualized in Fig. 4 a five-terminal grid based on a modified part of the CIGRÉ HVDC Test System with subsea cable sections (adapted insulation thickness $C' = 0.152$ μF/km) and overhead lines is investigated, see [28]. A dc–dc converter is not considered since this is beyond the scope of this work. The corresponding set of fundamental parameters is listed in Table I. Terminal MMC C2 and MMC D1 are connected to DFIG wind farm arrays and absorb the generated power. The three remaining converters located on the mainland are connected to ac grids and MMC B1 and MMC B2 participate in active dc grid primary control tasks according to their assigned role, see Table II. DC and ac lines or cables are represented with a π-equivalent. Gains for the current and energy proportional-integral (PI) controllers are initialized by considering further information provided in [10] and [16]. The corresponding control loops are given in Sections III and IV. In addition, all relevant measurement delays as well as the FIR filters have to be considered. All phase module current dynamics are adjusted to improve the transient dc network behavior and are listed in Table I.

TABLE I
Five-Terminal Test System Parameter Set

Main Parameters	**Value**
Nominal DC voltage	+/- 500 kV
Nominal mainland / offshore AC voltage	380 kV / 150 kV
Transformer Parameters	**Value**
Onshore / Offshore Type Dy	380-380 kV / 220-150 kV
Leakage impedance / Resistance	0.16 pu / 0.056 pu
Converter Parameters	**Value**
SM number per arm / capacitor	520 / 10.6 mF
SM / arm sum capacitor voltage	2307 V / 1.2 MV
Arm inductance	50mH
Converter control / measurement delay	50 μs / 100 μs
Energy Controller Gains	**k_p / k_i gain**
Vertical balancing ($u^{\Sigma}_{\Delta,\alpha\beta 0}$)	$3.90{\cdot}10^{-3}$ / 0
Horizontal balancing ($u^{\Sigma}_{\Sigma,\alpha\beta}$)	$2.44{\cdot}10^{-3}$ / 0
Total balancing ($u^{\Sigma}_{\Sigma,0}$)	$2.44{\cdot}10^{-3}$ / $3.66{\cdot}10^{-2}$
Phase Module Controller Gains	**k_p / k_i gain**
Current phase module ($i_{\mathrm{phm},\alpha\beta}$)	25 / 7.22
Current phase module ($i_{\mathrm{phm},0}$)	see Fig. 4

TABLE II
Converter Control Mode

Converter	**Mode**
B2	DC voltage with power limit
B1	Deadband droop / margin 3%
A1	Constant power
C2 / D1	Offshore rectifier

B. Wind Farm Outage

In Fig. 5(a) and (b), the transient response of the five-terminal dc grid to a wind array outage (ac circuit breaker opens) connected to terminal MMC C2 at $t = 3.0$ s is shown. The faulted converter adjusts its power output and returns to the initial arm sum voltage setpoint, see Fig. 5(c). The constant dc voltage-controlled MMC B2 is limited to a maximum ac power extraction of 910 MW, so the corresponding dc infeed is readjusted at around $t = 3.05$ s to remain as the converter energy above the critical limit. Caused by this power readjustment, the dc grid voltage level further decreases and MMC B1 leaves the 3% deadband

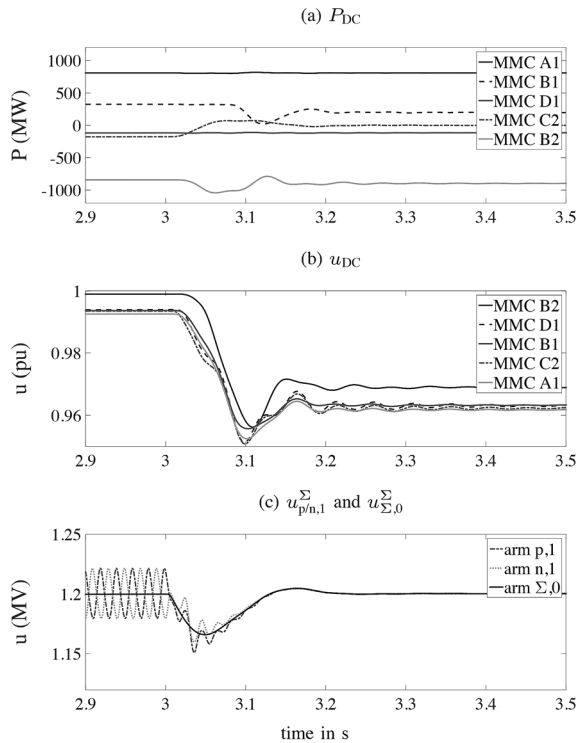

Fig. 5. Five-terminal MMC grid response to a wind farm outage at terminal MMC C2: (a) DC power output. (b) DC voltages. (c) Converter arm sum voltages of phase one and total sum voltage zero component of MMC C2.

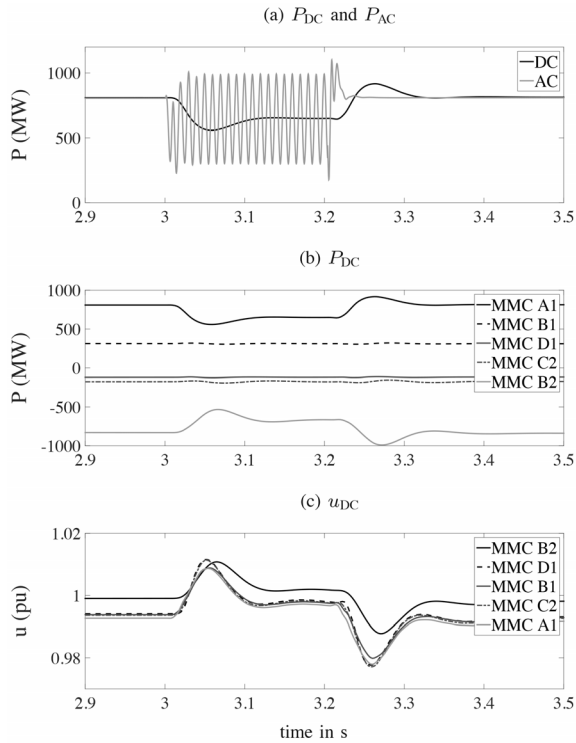

Fig. 6. Five-terminal MMC grid response to a line-to-ground fault at the PCC of MMC A1: (a) DC and ac power output of MMC A1, (b) dc power output, (c) dc voltages: (a) P_{DC} and P_{AC}, (b) P_{DC}, and (cu_{DC}.

at around $t = 3.08$ s and contributes to the grid power balance with a sensitivity of 35 MW/kV in the following time period.

C. Single-Phase Fault

At the PCC of terminal MMC A1, a line-to-ground fault, which is cleared after 200 ms, is applied at $t = 3$ s. Fig. 6(a) shows the converter ac- and dc-side active power output. The ac power controller keeps the output currents limited and balanced since negative-sequence voltage components are fed in directly from the MCCF. To keep the remaining total converter energy stable, the dc current is reduced and redistributed between the three-phase modules. This is affecting the dc grid voltages caused by a sudden power drop, see Fig. 6(b) and (c). The dc voltage-controlled converter MMC B2 is capable of following the steady-state setpoint deviation and rebalances input and output power of the multiterminal system during and after the fault. Due to the average energy control and the decoupled current systems, previously shown power oscillations with double-line frequency do not reach the dc-side quantities; in other words, a converter acts like a firewall. Fig. 7 shows the converter internal sum voltage and phase module current quantities. The power ripple is buffered within the distributed capacitor energy storage of MMC A1, see increased arm sum voltage ripple in Fig. 7(a). Furthermore, as shown in Fig. 7(b) and (c), the phase module current adjustment at the faulted terminal MMC A1 as well as the selected sum voltage quantities of MMC terminal B2 are shown.

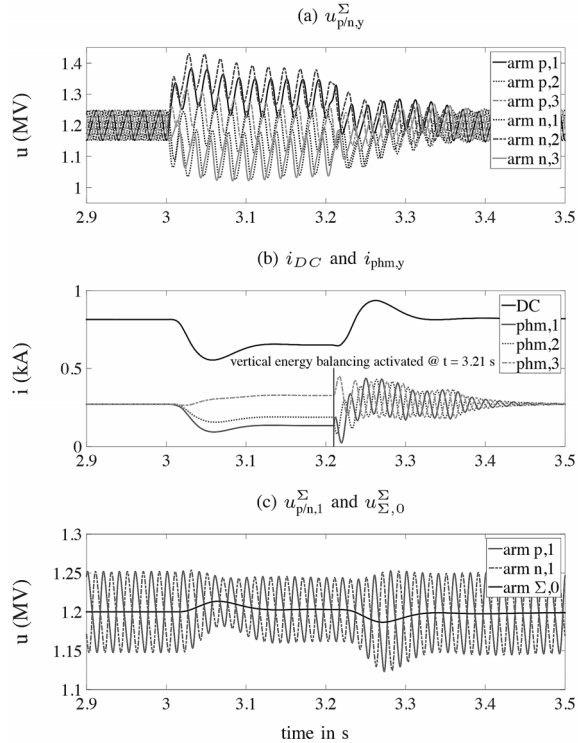

Fig. 7. Five-terminal MMC grid response to a line-to-round fault at the PCC of MMC A1: (a) converter arm sum voltages of MMC A1, (b) dcnd phase module current of MMC A1, and (c) converter arm sum voltages of phase one and total sum voltage zero component of MMC B2. (a) $u^{\Sigma}_{\mathrm{p/n,y}}$, (b) i_{DC} and $i_{\mathrm{phm,y}}$, and (c) $u^{\Sigma}_{\mathrm{p/n,1}}$ and $u^{\Sigma}_{\Sigma,0}$.

VII. Conclusion

In this paper, a simulation framework for MMC-based multiterminal HVDC systems is presented. The selected modeling concept offers insight into global arm quantities, considered as essential parameters to investigate transient system controllability. Besides the feature to handle unbalanced voltage conditions in one of the interfaced ac networks, this control approach facilitates active regulation strategies of all converter arm energies to keep the system within a predefined operating area during and subsequent to dynamic events. In particular, the possibility to resume to an initially set energy distribution within each converter terminal offers a wide range of novel evaluation opportunities. These are dc grid control and their interplay with offshore wind capacities, transient response to ac grid frequency deviations, and active handling of ac harmonics, handling of power fluctuations without causing ac–dc interactions, and influence analysis of energy-storage layout on ac–dc interaction suppressing capabilities. The results based on a five-terminal system in Matlab/Simulink validate the universal applicability.

References

[1] G. Asplund *et al.*, "HVDC grid feasibility study," Paris, France, Tech. Rep., Apr. 2013, CIGRÉ TB533 (WG B4.52).

[2] N. Ahmed, A. Haider, D. Van Hertem, L. Zhang, and H.-P. Nee, "Prospects and challenges of future HVDC supergrids with modular multilevel converters," in *Proc. 14th Eur. Conf. Power Electron. Appl.*, Birmingham, U.K., Aug. 2011, pp. 1–10.

[3] O. D. Adeuyi, N. Jenkins, and J. Wu, "Topologies of the north sea supergrid," in *Proc. 48th Int. Univ. Power Eng. Conf.*, Dublin, Ireland, Sep. 2013, pp. 1–6.

[4] A. Lesnicar and R. Marquardt, "An innovative modular multilevel converter topology suitable for a wide power range," in *Proc. IEEE Power Tech Conf.*, Bologna, Italy, Jun. 2003, vol. 3, pp. 1–6.

[5] J. Beerten, O. Gomis-Bellmunt, X. Guillaud, J. Rimez, A. van der Meer, and D. van Hertem, "Modeling and control of HVDC grids: A key challenge for future power systems," presented at the 18th Power System Comput. Conf., Wroclaw, Poland, Aug. 2014.

[6] S. Dennetière, H. Nguefeu, H. Saad, and J. Mahseredjian, "Modeling of modular multilevel converters for the France-Spain link," presented at the Int. Conf. Power Syst. Transients, Vancouver, BC, Canada, 2013.

[7] A. Beddard, M. Barnes, and R. Preece, "Comparison of detailed modeling techniques for MMC employed on VSC-HVDC schemes," *IEEE Trans. Power Del.*, vol. 30, no. 2, pp. 579–589, Apr. 2015.

[8] S. Rohner, S. Bernet, M. Hiller, and R. Sommer, "Modulation, losses, and semiconductor requirements of modular multilevel converters," *IEEE Trans. Ind. Electron.*, vol. 57, no. 8, pp. 2633–2642, Aug. 2010.

[9] Q. Tu and Z. Xu, "Impact of sampling frequency on harmonic distortion for modular multilevel converter," *IEEE Trans. Power Del.*, vol. 26, no. 1, pp. 298–306, Jan. 2011.

[10] J. Kolb, F. Kammerer, M. Gommeringer, and M. Braun, "Cascaded control system of the modular multilevel converter for feeding variable-speed drives," *IEEE Trans. Power Electron.*, vol. 30, no. 1, pp. 349–357, Jan. 2015.

[11] S. Debnath, J. Qin, B. Bahrani, M. Saeedifard, and P. Barbosa, "Operation, control, and applications of the modular multilevel converter: A review," *IEEE Trans. Power Electron.*, vol. 30, no. 1, pp. 37–53, Jan. 2015.

[12] P. Munch, D. Gorges, M. Izak, and S. Liu, "Integrated current control, energy control and energy balancing of modular multilevel converters," in *Proc. 36th Annu. Conf. IEEE Ind. Electron. Soc.*, Phoenix, AZ, USA, Nov. 2010, pp. 150–155.

[13] S. Rohner, J. Weber, and S. Bernet, "Continuous model of modular multilevel converter with experimental verification," in *Proc. IEEE Energy Convers. Congr. Expo.*, Phoenix, AZ, USA, Sep. 2011, pp. 4021–4028.

[14] M. Dommaschk, Modularer multilevelstromrichter fuer anwendungen in der hochspannungsgleichstrombertragung Ph.D. dissertation, Dept. Elect. Eng., Chemnitz Univ. of Technology. Chemnitz, Germany, 2013.

[15] Q. Tu, Z. Xu, Y. Chang, and L. Guan, "Suppressing dc voltage ripples of MMC-HVDC under unbalanced grid conditions," *IEEE Trans. Power Del.*, vol. 27, no. 3, pp. 1332–1338, Jul. 2012.

[16] M. Guan and Z. Xu, "Modeling and control of a modular multilevel converter-based HVDC system under unbalanced grid conditions," *IEEE Trans. Power Electron.*, vol. 27, no. 12, pp. 4858–4867, Dec. 2012.

[17] J.-W. Moon, C.-S. Kim, J.-W. Park, D.-W. Kang, and J.-M. Kim, "Circulating current control in MMC under the unbalanced voltage," *IEEE Trans. Power Del.*, vol. 28, no. 3, pp. 1952–1959, Jul. 2013.

[18] J.-W. Moon, J.-W. Park, D.-W. Kang, and J.-M. Kim, "A control method of HVDC-modular multilevel converter based on arm current under the unbalanced voltage condition," *IEEE Trans. Power Del.*, vol. 30, no. 2, pp. 529–536, Apr. 2015.

[19] L. Harnefors, A. Antonopoulos, S. Norrga, L. Angquist, and H.-P. Nee, "Dynamic analysis of modular multilevel converters," *IEEE Trans. Ind. Electron.*, vol. 60, no. 7, pp. 2526–2537, Jul. 2013.

[20] H. Saad, J. Peralta, S. Dennetiere, J. Mahseredjian, J. Jatskevich, J. Martinez, A. Davoudi, M. Saeedifard, V. Sood, X. Wang, J. Cano, and A. Mehrizi-Sani, "Dynamic averaged and simplified models for MMC-based HVDC transmission systems," *IEEE Trans. Power Del.*, vol. 28, no. 3, pp. 1723–1730, Jul. 2013.

[21] J. Xu, C. Zhao, W. Liu, and C. Guo, "Accelerated model of modular multilevel converters in pscad/emtdc," *IEEE Trans. Power Del.*, vol. 28, no. 1, pp. 129–136, Jan. 2013.

[22] X. Guo, W. Wu, and Z. Chen, "Multiple-complex coefficient-filter-based phase-locked loop and synchronization technique for three-phase grid-interfaced converters in distributed utility networks," *IEEE Trans. Ind. Electron.*, vol. 58, no. 4, pp. 1194–1204, Apr. 2011.

[23] S. Golestan, M. Monfared, and F. Freijedo, "Design-oriented study of advanced synchronous reference frame phase-locked loops," *IEEE Trans. Power Electron.*, vol. 28, no. 2, pp. 765–778, Feb. 2013.

[24] C. Barker and R. Whitehouse, "Further developments in autonomous converter control in a multi-terminal HVDC system," in *Proc. 10th IET Int. Conf. AC DC Power Transm.*, Birmingham, 2012, pp. 215–220.

[25] T. K. Vrana, J. Beerten, R. Belmans, and O. B. Fosso, "A classification of DC node voltage control methods for HVDC grids," *Elect. Power Syst. Res.* vol. 103, pp. 137–144, Oct. 2013. [Online]. Available: http://www.sciencedirect.com/science/article/pii/S0378779613001193

[26] S. Wenig, Y. Rink, and T. Leibfried, "Multi-terminal HVDC control strategies applied to the cigre B4 DC grid test system," in *Proc. 49th Int. Univ. Power Eng. Conf.*, Cluj, Romania, Sep. 2014, pp. 1–6.

[27] S. Cole, J. Beerten, and R. Belmans, "Generalized dynamic VSC MTDC model for power system stability studies," *IEEE Trans. Power Syst.*, vol. 25, no. 3, pp. 1655–1662, Aug. 2010.

[28] T. Vrana, Y. Yang, D. Jovcic, S. Dennetière, J. Jardini, and H. Saad, "The CIGRÉ B4-DC grid test system," CIGRÉ WG B4.57 and B4.58. Paris, France., 2013. [Online]. Available: http://b4.cigre.org/Publications/Documents-related-to-the-development-of-HVDC-Grids

[29] C. Feltes and I. Erlich, "Variable frequency operation of DFIG based wind farms connected to the grid through VSC-HVDC link," in *Proc. IEEE Power Eng. Soc. Gen. Meeting*, Tampa, FL, USA, Jun. 2007, pp. 1–7.

[30] O. Gomis-Bellmunt, A. Egea-Alvarez, A. Junyent-Ferre, J. Liang, J. Ekanayake, and N. Jenkins, "Multiterminal HVDC-VSC for offshore wind power integration," in *Proc. IEEE Power Energy Soc. Gen. Meeting*, Detroit, MI, USA, Jul. 2011, pp. 1–6.

[31] I. Erlich, F. Shewarega, C. Feltes, F. Koch, and J. Fortmann, "Offshore wind power generation technologies," *Proc. IEEE*, vol. 101, no. 4, pp. 891–905, Apr. 2013.

[32] A. Timofejevs, D. Gamboa, M. Liserre, R. Teodorescu, and S. Chaudhary, "Control of transformerless MMC-HVDC during asymmetric grid faults," in *Proc. IEEE 39th Annu. Ind. Electron. Soc. Conf.*, Vienna, Austria, Nov. 2013, pp. 2016–2021.

Simon Wenig (S'15) was born in Coburg, Germany, in 1985. He received the Dipl.-Ing. degree in electrical engineering from the Karlsruhe Institute of Technology, Karlsruhe, Germany, in 2013, where he is currently pursuing the Ph.D. degree in electrical engineering.

His research interests include HVDC grids, MMC modeling and control, as well as RES integration.

Mr. Wenig is a member of VDE and CIGRE.

Freiber Rojas was born in Caracas, Venezuela, in 1991. He received the Ingenieŕıa Eĺectrica degree from Simon Bolivar University, Venezuela, in 2015.

His research interests include HVDC grids, and MMC operation under unbalanced voltage conditions.

Kevin Schönleber (S'14) was born in Mannheim, Germany, in 1986. He received the Dipl.-Ing. degree in electrical engineering from the Karlsruhe Institute of Technology, Karlsruhe, Germany, in 2013, and is currently pursuing the Ph.D. degree in operation and control of dc-connected offshore wind power plants in the MEDOW research project at the Universitat Politecnica de Catalunya, Barcelona, Spain.

Currently, he is a Marie Curie Early-Stage Researcher at Alstom Renewable Power. His research interests include the operation of offshore wind power plants, HVDC, and power quality.

Michael Suriyah (M'14) was born in Kuala Lumpur, Malaysia, in 1982. He received the diploma and M.Sc. degrees in electrical engineering from the University of Applied Sciences, Karlsruhe, Germany, in 2007 and 2008, respectively, and the Ph.D. degree in electrical engineering from the Karlsruhe Institute of Technology, Karlsruhe, Germany, in 2013.

Currently, he is the Head of the Department for Power Networks at the Institute of Electric Energy Systems and High-Voltage Technology. His research interests include aging diagnostics and onsite testing of power transformers, high-voltage testing methods, analysis of electric power networks, as well as planning of future power systems.

Dr. Suriyah is a member of VDE.

Thomas Leibfried (M'96) was born in Neckarsulm, Germany, in 1964. He received the Dipl.-Ing. and Dr.-Ing. degrees from the University of Stuttgart, Stuttgart, Germany, in 1990 and 1996, respectively.

From 1996 to 2002, he was with the Siemens AG, Nuremberg, Germany, working in the power transformer business in various technical and management positions. In 2002, he joined the University of Karlsruhe, Karlsruhe, Germany, as Head of the Institute of Electric Energy Systems and High-Voltage Technology. He is a member of VDE and CIGRE.